AIAA JOURNAL
Vol. 32, No. 10, October 1994

Active Control of Wake/Blade-Row Interaction Noise

Kenneth A. Kousen* and Joseph M. Verdon†
United Technologies Research Center, East Hartford, Connecticut 06108

This paper describes an analytical/computational approach for controlling the noise generated by wake/blade-row interaction through the use of antisound actuators on the blade surfaces. A representative two-dimensional section of a fan stage, composed of an upstream fan rotor and a downstream fan exit guide vane (FEGV), is examined. An existing model for the wakes generated by the rotor is analyzed to provide realistic magnitudes for the vortical excitations imposed at the inlet to the FEGV. The acoustic response of the FEGV is determined at multiples of the blade passing frequency by using the linearized unsteady flow analysis, LINFLO. An analysis then is presented to determine the complex amplitudes required for the control surface motions to best reduce the far-field noise. The effectiveness of the control is measured by the decrease in the circumferentially averaged sound pressure level, which is minimized by a standard least-squares procedure.

I. Introduction

WAKE/blade-row interactions in turbofan engines produce discrete tones at multiples of the blade passing frequency (BPF), whose magnitudes are significantly higher than the associated broadband noise levels.[1] Current trends toward higher bypass ratios and shorter duct lengths in modern engines emphasize the discrete tone contributions while reducing the effectiveness of passive noise control using acoustic liners.[2] Consequently, active noise control techniques are receiving attention as a possible approach to reduce the discrete tone noise levels.

Active control of noise is an important area of research,[3–7] but applications to the turbofan engine noise problem have begun to appear only recently[1,2,8] Methods for minimizing noise have concentrated on either reducing the magnitude of sound generated at the source[1,8] or generating an antisound field to cancel the undesired acoustic response modes.[2] The present paper involves an attempt to combine these two approaches to reduce the noise by generating antisound using control actuators in close proximity to the noise source. It is hoped that by locating the control actuators directly on the stator blades, the required displacement amplitudes for effective noise cancellation will be reduced to physically useful levels.

To perform such an investigation, analyses are required to determine the magnitudes of representative wake excitations generated by the rotor, the acoustic responses of the stator row to these excitations, and the control surface oscillations that best reduce the acoustic response of the stator. Section II.A presents the method used to determine the complex amplitudes of the vortical excitations that model the rotor wakes as seen by the stator. The linearized unsteady cascade analysis, LINFLO,[9,10] reviewed in Sec. II.B, provides a means for determining the acoustic response of the stator to vortical excitations imposed at the inlet boundary, and Sec. III presents the control algorithms developed to reduce the undesired acoustic responses. Results of the combined investigation are presented in Sec. IV.

It is observed that if the number of independent control surface actuators is equal to the number of propagating acoustic response modes, then oscillation amplitudes of the actuators can be found that result in a complete elimination of the noise. Analyses are also provided, based on weighted least-squares minimization procedures, for reducing the noise as much as possible in the more general case where the number of propagating response modes exceeds the number of control surfaces. In each case, the required control surface displacement amplitudes are found to be between a few thousandths and a few ten-thousandths of stator chord, which suggests that active control of wake/blade-row interaction noise using blade-surface actuators may be a promising and useful approach.

Received Oct. 22, 1993; presented as Paper 93-4351 at the AIAA 15th Aeroacoustics Conference, Long Beach, CA, Oct. 25–27, 1993; revision received March 28, 1994; accepted for publication March 30, 1994.

*Research Engineer, Physical and Mathematical Modeling. Senior Member AIAA.

†Manager, Theoretical and Computational Fluid Dynamics. Associate Fellow AIAA.

II. Physical Problem

A two-dimensional representation of a typical fan stage consisting of an upstream fan or rotor and a downstream exit stator (FEGV) is shown in Fig. 1, along with the associated velocity triangles. For each row, inlet and exit flow quantities are indicated by the subscripts $\mp\infty$, respectively. The wheel velocity of the rotor is V_W. Total ($\tilde{V}$) and mean (V) velocity components are given with and without tildes, respectively. Where confusion between reference frames might occur, primes are used to denote quantities associated with the rotor frame. Unless otherwise noted, all lengths have been nondimensionalized with respect to the FEGV blade chord and all velocities with respect to the FEGV inlet freestream velocity.

Axial and circumferential distances are represented via the Cartesian coordinate systems (ξ', η') and (ξ, η), which are rigidly attached to the fan and FEGV rows. For the latter, the mean or steady-state positions of the blade chord lines coincide with the line segments $\eta = \xi \tan\Theta + mG$, $0 \le \xi \le \cos\Theta$, $m = 0, \pm1, \pm2, \ldots$, where m is a blade number index, Θ is the cascade stagger angle, and $\boldsymbol{G}$ is the gap vector directed along the η axis with magnitude equal to the blade spacing. Fan cascade quantities are defined analogously.

A. Wake Excitation Model

The goal of the wake analysis is to represent the rotor wakes as individual Fourier modes of vortical excitation that can be imposed at the inlet of the stator row. The complex amplitudes of the Fourier modes are determined through an analysis of the fan wakes and a transformation from rotor-fixed to stator-fixed coordinates. In the rotor frame, the flow within each wake is steady and assumed to be parallel and aligned with the mean exit flow direction. Each wake is characterized by a given velocity profile, centerline velocity defect $V'_{\min}/V'_e$, and wake half-width δ, which are defined later. The wakes have a circumferential period equal to the rotor gap G'. It is also assumed that across each wake the static pressure P' is constant. This assumption implies that the fan wakes will give rise to velocity disturbances that are purely rotational. Since it can be shown that the Cartesian components of the velocity disturbances associated with vorticity are not independent, it is sufficient to find the individual Fourier components of $\tilde{v} \cdot \boldsymbol{e}_N$, i.e., the component of

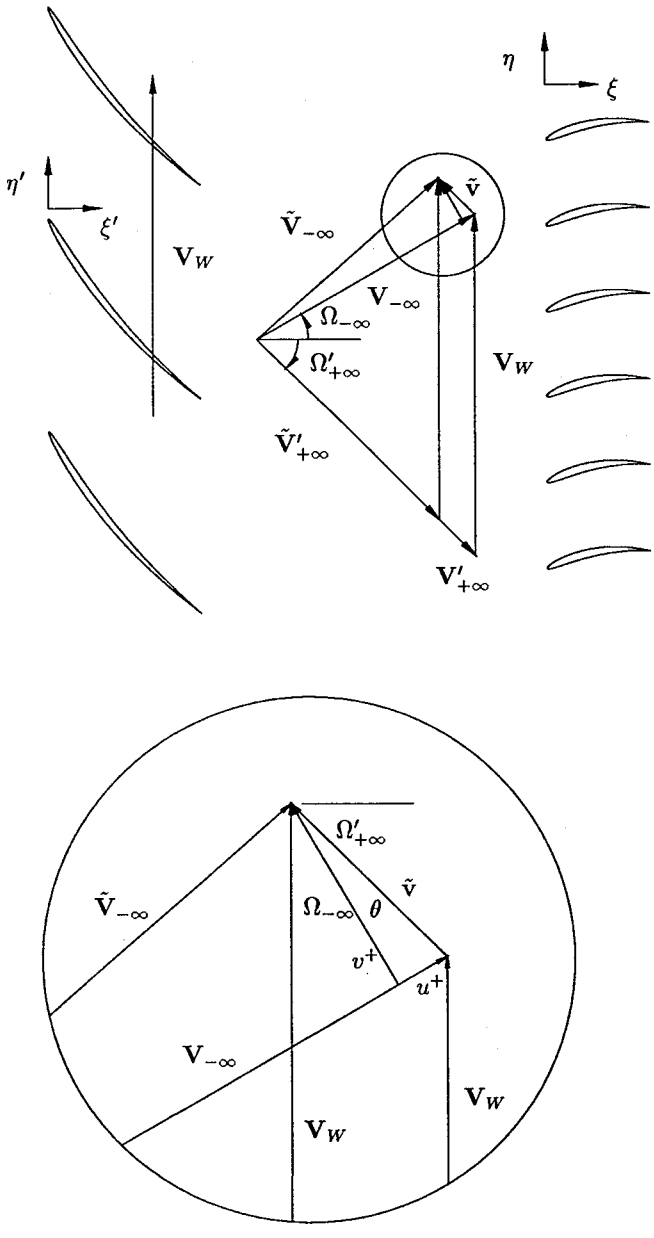

Fig. 1 Fan stage configuration, including velocity triangle and expanded detail.

the disturbance velocity normal to the inlet flow direction of the FEGV, at each multiple of BPF.

The velocity triangle between the rotor and stator rows implies that

$$\tilde{\boldsymbol{v}} = \tilde{\boldsymbol{V}}'_{+\infty} - \boldsymbol{V}'_{+\infty} \tag{1}$$

which represents the relationship between the disturbance velocity $\tilde{\boldsymbol{v}}$ and the total and mean velocities $\tilde{\boldsymbol{V}}'_{+\infty}$ and $\boldsymbol{V}'_{+\infty}$ from the rotor row. Consequently, the perturbation velocity can be found by an analysis of excitation row quantities alone.

The symbols v^+ and u^+ will be used to represent the components of $\tilde{\boldsymbol{v}}$ in directions normal and tangential to the stator inlet mean flow velocity. The component v^+ is given by

$$v^+ = \tilde{\boldsymbol{v}} \cdot \boldsymbol{e}_N = (V'_{+\infty} - \tilde{V}'_{+\infty}) \sin(\Omega'_{+\infty} - \Omega_{-\infty})$$

$$= \sum_{n=-\infty}^{\infty} v_n^+ \exp(in\kappa_\eta \eta') \tag{2}$$

where $\kappa_\eta = 2\pi/G'$ is the circumferential wave number, and

$$v_n^+ = \frac{1}{G'} \int_{\eta'_{\text{ref}}}^{\eta'_{\text{ref}}+G'} v^+(\eta') \exp(in\kappa_\eta \eta')\, d\eta' \tag{3}$$

where η'_{ref} is a reference location in the rotor frame.

The rotor-fixed and stator-fixed coordinates are related by $\boldsymbol{x}' = \boldsymbol{x} - \boldsymbol{V}_W t$, where $\boldsymbol{x}' = (\xi', \eta')$ is a position vector in the moving frame attached to the rotor and $\boldsymbol{x} = (\xi, \eta)$ is a position vector in the stationary reference frame. Inserting this coordinate transformation into Eq. (3) shows that the steady disturbance velocity in the rotating frame becomes a set of unsteady disturbance velocities in the stationary frame with frequencies $\omega_n = -n\kappa_\eta V_W$, where V_W is the wheel speed of the rotor.

The v_n^+ components are thus dependent upon the rotor exit velocity $\tilde{\boldsymbol{V}}'_{+\infty}$. This velocity is supplied through the semi-empirical rotor wake model of Majjigi and Gliebe,[11] which defines the wake velocity at streamwise locations downstream of the rotor in terms of a shape function, a centerline velocity defect, and a wake half-width.

In terms of the Cartesian coordinates (T', N') aligned with and normal to the rotor exit flow velocity and with origin at the rotor blade trailing edge, the velocity in a reference wake can be expressed as

$$V'(T', N') = V'_e(T')\left(1 - \frac{V'_{\text{def}}}{V'_{\text{min}}} \frac{V'_{\text{min}}}{V'_e}\right) \tag{4}$$

where $V'_e(T')$ is the velocity at the edge of a wake, $V'_{\text{def}}(T', N')$ is the wake velocity deficit, defined as the difference between the edge velocity and the velocity in the wake at each N', and $V'_{\text{min}}(T')$ is the minimum streamwise velocity across the wake. The quantity $V'_{\text{def}}/V'_{\text{min}} = f(N')$ is a shape function that is dependent only upon the normal coordinate N'. For simplicity, the wakes are assumed here to be symmetric, so that the minimum velocity occurs at the wake centerline and the quantity V'_{min}/V'_e will be hereafter referred to as the centerline velocity defect. A given wake velocity distribution is made unique by specifying the shape function, the centerline velocity defect, and the wake half-width, which is defined as the perpendicular distance between the points at which the wake deficit is half its maximum value. The shape function assumed here is a hyperbolic secant profile, given by

$$f(N') = \operatorname{sech}\left[\frac{2}{\delta}(\cosh^{-1}2)N'\right] \tag{5}$$

The centerline defect V'_{min}/V'_e and the half-width δ are given by the empirically determined functions[11]

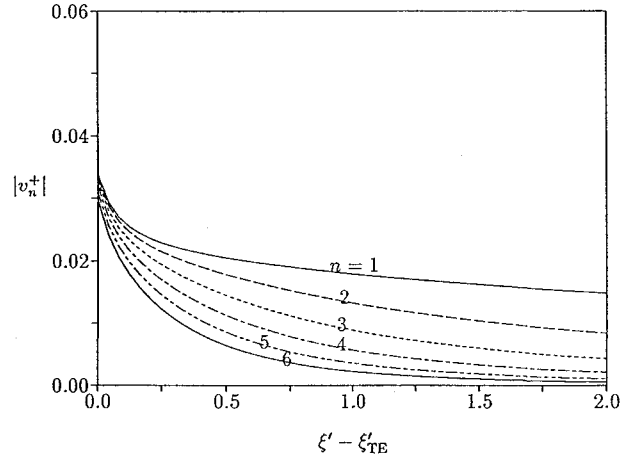

Fig. 2 Variation of the magnitudes of the complex Fourier components $|v_n^+|$ with axial distance ξ downstream of the trailing edge of the fan rotor.

$$\frac{V'_{\min}}{V'_e} = C_D^{1/4}\left(\frac{0.3675T' + 1.95}{7.65T' + 1.0}\right) \tag{6}$$

and

$$\delta = \frac{0.2375C_D^{1/8}T' + 0.034125}{0.357C_D^{1/8}T' + 1.0} \tag{7}$$

where C_D is the section drag coefficient. In these equations, the streamwise distance T' and the wake half-width δ have been nondimensionalized by the rotor chord.

For the cases discussed in this paper, values for the $|v_n^+|$ at several axial stations between the fan rotor and FEGV are shown in Fig. 2. The results in the figure used the values $V'_{\min}/V'_e = 0.55, \delta = 0.288$, and $C_D = 0.032$. This case is discussed further in Sec. IV. Note that there is an initial decay in the magnitude of each component, followed by a more gradual decrease with axial distance. Also, the initial decay is more pronounced for the higher order components. Common practice suggests that the axial spacing between the rotor trailing edges and the stator leading edges is a reasonable choice for evaluation of the v_n^+ values and will be adopted here. Figure 2 suggests that if this axial spacing is sufficiently large, the magnitudes of the Fourier components will not vary substantially.

B. Stator Row Acoustic Response

The acoustic response of the stator row to both vortical excitations and control surface oscillations is found using the LINFLO analysis.[9-10] The flow through the FEGV is considered to be a time-dependent, adiabatic, attached subsonic flow, with negligible body forces, of an inviscid non-heat-conducting perfect gas. It is assumed that in the absence of unsteady excitation the mean flow is uniform at the inlet to the FEGV. All excitations are assumed to be of small amplitude, periodic in time, and periodic in the circumferential or η direction.

Excitations are provided by the vortical disturbances described in the previous section and control surface oscillations, which are modeled as prescribed motions of the form

$$\mathcal{R}_B(x + mG, t) = \mathrm{Re}\{\boldsymbol{r}(x)\exp[i(\omega t + m\sigma)]\} \tag{8}$$

where $\boldsymbol{x}$ is restricted to specified sections of the reference ($m = 0$) blade surface B. Here $\mathcal{R}_B$ measures the displacement of a point on a blade surface relative to its mean or steady-state position, $\boldsymbol{x}$ is a position vector, $\boldsymbol{r}$ is a complex displacement-amplitude vector, σ is the interblade phase angle, and Re{} denotes the real part of a complex quantity.

Since the vortical and control surface oscillations are assumed to be of small amplitude, the nonlinear differential equations governing the fluid motion can be linearized about an underlying mean or steady flow. The first-order linearized flow properties are then harmonic in time at the temporal frequency ω of the specified excitation. The first-order unsteady fluctuations that arise from independent modes of excitation are not coupled, and so solutions for arbitrary disturbances can be obtained by superposition.

Blade-to-blade and phase-lagged periodicity require that the mean and first-order unsteady flow satisfy conditions of the form $\boldsymbol{V}(\boldsymbol{x} + m\boldsymbol{G}) = \boldsymbol{V}(\boldsymbol{x})$ and $\boldsymbol{v}(\boldsymbol{x} + m\boldsymbol{G}) = \boldsymbol{v}(\boldsymbol{x})\exp(im\sigma)$, respectively. Analytical far-field solutions can also be determined[12] and in combination with blade-to-blade periodicity reduce the computational solution domain to a single blade-passage region of the cascade of finite extent in the axial flow direction.

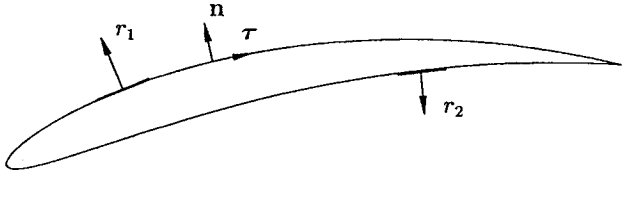

Fig. 3 Actuator implementation, with blade normal and tangential coordinate vectors shown.

Table 1 Interblade phase angles, frequencies, and complex amplitudes for the first three harmonics of the vortical excitation calculated from the wake model

	Vortical excitation data		
n	σ_n	ω_n	v_n^+
1	−2.513	4.106	$(0.14807 \times 10^{-1}, 0)$
2	−5.026	8.212	$(0.82745 \times 10^{-2}, 0)$
3	−7.539	12.318	$(0.41493 \times 10^{-2}, 0)$

The steady background flow is taken to be isentropic and irrotational. Thus $\boldsymbol{V} = \nabla\Phi$, and the governing partial differential equation for the mean flow is

$$\nabla \cdot (\bar{\rho}\nabla\Phi) = 0 \tag{9}$$

The momentum and state equations under these assumptions imply that the fluid properties are related by

$$(M_{-\infty}A)^2 = 1 - \frac{\gamma - 1}{2}M_{-\infty}^2[(\nabla\Phi)^2 - 1] = \bar{\rho}^{\gamma-1} = (\gamma M_{-\infty}^2 P)^{(\gamma-1)/\gamma} \tag{10}$$

where Φ, M, A, $\bar{\rho}$, and P are the steady velocity potential, Mach number, speed of sound propagation, density, and pressure, respectively, and γ is the specific heat ratio of the fluid. Numerical procedures for determining two-dimensional steady potential flows through cascades have been developed extensively (e.g., see Ref. 13), particularly for flows with subsonic relative inlet and exit Mach numbers ($M_{\mp\infty} < 1$). Equation (9) is solved subject to prescribed uniform inflow conditions, flow tangency at the blade surfaces, and a Kutta condition at the blade trailing edges.

For an isentropic unsteady flow, the system of first-order linearized field equations reduces to

$$\frac{\bar{D}\boldsymbol{v}_R}{Dt} + (\boldsymbol{v}_R \cdot \nabla)\nabla\Phi = 0 \tag{11}$$

and

$$\frac{\bar{D}}{Dt}\left(A^{-2}\frac{\bar{D}\phi}{Dt}\right) - \bar{\rho}^{-1}\nabla\cdot(\bar{\rho}\nabla\phi) = \bar{\rho}^{-1}\nabla\cdot(\bar{\rho}\,\boldsymbol{v}_*) \tag{12}$$

where the complex amplitude of the unsteady velocity $\boldsymbol{v}$ has been decomposed into a rotational part $\boldsymbol{v}_R$, an irrotational part written as $\nabla\phi$, the gradient of a convected or pressureless potential $\nabla\phi_*$, and $\boldsymbol{v}_* = \boldsymbol{v}_R + \nabla\phi$. The quantity $\bar{D}/Dt = i\omega + \boldsymbol{V}\cdot\nabla$ is a convective derivative based on the mean flow velocity. Closed-form solutions can be determined for the rotational velocity fluctuations[10,14] and for the convected potential[10,15] ϕ_* in terms of the drift and stream functions of the steady background flow.

To complete the formulation of the unsteady flow problem, boundary conditions are required along the blade and wake surfaces, as well as at the far-field boundaries. Flow tangency is required along the blade surfaces, jump conditions are specified at vortex-sheet unsteady wakes, and information regarding the uniform mean flow at inlet and exit and any vortical fluctuations at inlet must be specified. The flow tangency condition is given by

$$\nabla\phi\cdot\boldsymbol{n} = [i\omega\boldsymbol{r} + (\nabla\phi\cdot\tau)(\tau\cdot\nabla)\boldsymbol{r} - (\boldsymbol{r}\cdot\nabla)\nabla\phi]\cdot\boldsymbol{n} \tag{13}$$

where $\boldsymbol{n}$ and τ are unit vectors normal and tangential to the mean blade surfaces B_m, as shown in Fig. 3. The jump conditions are

$$[\![\bar{D}\phi/Dt]\!] = 0 \quad \text{and} \quad [\![\nabla\phi]\!]\cdot\boldsymbol{n} = 0 \tag{14}$$

and are applied along the mean blade wakes. Analytical far-field boundary conditions are derived in Ref. 12, which allow outgoing

acoustic disturbances either to attenuate with axial distance from the blade row or to propagate through the mesh boundaries without reflection. The analytic solutions in Ref. 12 presume that the far-field acoustic response is governed by a two-dimensional convected wave equation. This condition is satisfied provided the combination of the hub-to-duct radius ratio of the fan/FEGV stage and the frequencies of the excitations do not cause any high-order radial acoustic modes to propagate.

The boundary value problem for the unsteady flow thus reduces to the numerical solution of Eq. (12) subject to the flow tangency condition of Eq. (13), the jump conditions of Eq. (14), any specified far-field or control surface excitations, and the analytic far-field boundary conditions. Details of the formulation and solution procedure can be found in Refs. 9 and 10.

The resultant acoustic responses to the vortical excitations provide the targets of the active control analysis.

III. Control Surface Analysis

In this section, the implementation of the blade surface actuators and the determination of the oscillation amplitudes required to best minimize the noise in the far field of the FEGV are described. Note that, for the purposes of the control analysis, acoustic response modes of the same circumferential order but traveling in different directions are considered to be independent modes, even though they have the same frequency and circumferential wave number.

A. Antisound Actuators

The control surface actuators, or pistons, have been implemented into the LINFLO analysis as oscillating surfaces on the suction and pressure surfaces of each blade in the cascade. The net displacement of the actuators is represented by Eq. (8), where the complex amplitude of the displacement at the reference ($m = 0$) blade is given by

$$\boldsymbol{r}(x) = \sum_{k=1}^{K} \boldsymbol{r}_k [U(\boldsymbol{x} - \boldsymbol{x}_{k,le}) - U(\boldsymbol{x} - \boldsymbol{x}_{k,te})] \tag{15}$$

for a set of K control surfaces or pistons, where $\boldsymbol{r}_k = r_k \boldsymbol{n}$ is the displacement of the kth piston with complex amplitude r_k, U is the unit step function, and $\boldsymbol{x}_{k,le}$ and $\boldsymbol{x}_{k,te}$ are the locations of the leading and trailing edges of the kth piston. Figure 3 shows a typical example of the piston implementation, with one actuator on the suction surface and one on the pressure surface of an FEGV blade. Individual pistons are specified by choosing midpoint locations and lengths as a fraction of chord. The control analysis then calculates chordwise positions of the leading and trailing edges of the piston and requires the blade surface segment within this range to perform a translational oscillation normal to the blade surface at a specified frequency and complex amplitude.

The analysis presented later shows how to determine the complex amplitudes of the pistons to best minimize the noise, given the piston lengths and locations. The analysis assumes that there are K actuators on each blade, whose motions at each chordwise position on nonreference blades are related to their counterparts on the reference blade through the blade-to-blade and phase-lagged periodicity conditions.

B. Control Algorithm

The control algorithm is based on the superposition principle. The acoustic responses due to the oscillations of the control surfaces are calculated, and the complex amplitudes of the control surface motions are adjusted until their combined responses minimize the undesired noise. Since the equations governing the unsteady responses are linear, the required control surface displacements are found from a solution of a linear system of equations.

Assume that there are N acoustic response modes and K independent control surfaces. In the following examples, the acoustic response modes are restricted to those of propagating type, but this is not mandatory. The complex amplitudes of the acoustic response modes can be collected into a net acoustic response vector $\boldsymbol{p}_R$, which is composed of responses due to the vortical excitation $\boldsymbol{p}_{R,\text{exc}}$ and responses due to the control surface motions $\boldsymbol{p}_{R,\text{ctrl}}$, i.e.,

$$\boldsymbol{p}_R = \boldsymbol{p}_{R,\text{exc}} + \boldsymbol{p}_{R,\text{ctrl}} = \boldsymbol{p}_{R,\text{exc}} + \boldsymbol{A}\boldsymbol{r} \tag{16}$$

The $N \times K$ matrix $\boldsymbol{A}$ contains as its elements the complex amplitudes of each acoustic response wave resulting from a unit amplitude oscillation of each control surface, and the vector $\boldsymbol{r}$ contains the complex amplitudes r_k of the control surface motions. If $K = N$, the matrix $\boldsymbol{A}$ is square and invertible. Consequently, a set of control surface amplitudes given by

$$\boldsymbol{r}_{\text{exact}} = -\boldsymbol{A}^{-1}\boldsymbol{p}_{R,\text{exc}} \tag{17}$$

will yield $\boldsymbol{p}_R = 0$. In this case, the amplitude of each propagating acoustic response wave will be zero.

If, however, $K < N$, then the length of the net acoustic response vector $\|\boldsymbol{p}_R\| = (\boldsymbol{p}_R^H \cdot \boldsymbol{p}_R)^{1/2}$, where the superscript H denotes the Hermetian or conjugate transpose, provides a natural measure of the net sound. To minimize $\|\boldsymbol{p}_R\|$ in a least-squares sense, it can be shown[16] that it is necessary to choose the vector $\boldsymbol{p}_{R,\text{ctrl}} = \boldsymbol{A}\boldsymbol{r}$ to be perpendicular to $\boldsymbol{p}_R$, i.e.,

$$\boldsymbol{p}_{R,\text{ctrl}}^H \cdot \boldsymbol{p}_R = (\boldsymbol{A}\boldsymbol{r})^H (\boldsymbol{A}\boldsymbol{r} + \boldsymbol{p}_{R,\text{exc}}) = 0 \tag{18}$$

Expanding the Hermetian product allows this equation to be written as

$$\boldsymbol{r}^H (\boldsymbol{A}^H\boldsymbol{A}\boldsymbol{r} + \boldsymbol{A}^H\boldsymbol{p}_{R,\text{exc}}) = 0 \tag{19}$$

whose nontrivial solution is

$$\boldsymbol{r}_{\text{lsq}} = -(\boldsymbol{A}^H\boldsymbol{A})^{-1}\boldsymbol{A}^H\boldsymbol{p}_{R,\text{exc}} \tag{20}$$

The elements r_k of $\boldsymbol{r}_{\text{lsq}}$ are the complex amplitudes of the desired set of control surface displacements.

The least-squares minimization treats each element of the propagating response vector as equally important. It may be true in certain situations that the reduction of some modes is more important than others. Consequently, a weighting matrix $\boldsymbol{W}$ can be introduced into Eq. (16), i.e., we can write

$$\boldsymbol{W}\boldsymbol{p}_R = \boldsymbol{W}\boldsymbol{p}_{R,\text{exc}} + \boldsymbol{W}\boldsymbol{A}\boldsymbol{r} \tag{21}$$

The matrix $\boldsymbol{W}$ is chosen to be square, diagonal, and composed of real elements. The values specified on the diagonal represent the relative importance assigned to the individual modes, whereas any off-diagonal elements represent coupling between the modes. The least-squares solution of this equation minimizes the length of a weighted net response vector $\|\boldsymbol{W}\boldsymbol{p}_R\|$ and is given by

$$\boldsymbol{r}_{w\text{lsq}} = -(\boldsymbol{A}^H\boldsymbol{W}^T\boldsymbol{W}\boldsymbol{A})^{-1}\boldsymbol{A}^H\boldsymbol{W}^T\boldsymbol{W}\boldsymbol{p}_{R,\text{exc}} \tag{22}$$

Note that if the matrix $\boldsymbol{A}$ is invertible, then Eq. (22) reduces to the solution given in Eq. (17). The least-squares solution given in Eq. (20) represents the case where the weighting matrix is chosen to be the identity matrix. This procedure minimizes the length of a weighted net response vector $\|\boldsymbol{W}\boldsymbol{p}_R\|$, which could result in a larger value for $\|\boldsymbol{p}_R\|$ than in cases without control applied.

C. Sound Pressure Level

To give some physical relevance to the magnitude of the net acoustic response vector $\|\boldsymbol{p}_R\|$, we relate it to the circumferentially averaged sound pressure level $\overline{SPL}$. The sound pressure level SPL is defined to be

$$SPL = 20 \log_{10} \frac{p_{\text{rms}}}{p_{\text{ref}}} \tag{23}$$

where p_{rms} is the root mean square value of the unsteady pressure, and p_{ref} is a reference pressure whose dimensional value is generally taken to be 2×10^{-5} Pa for airborne sound. The mean-square

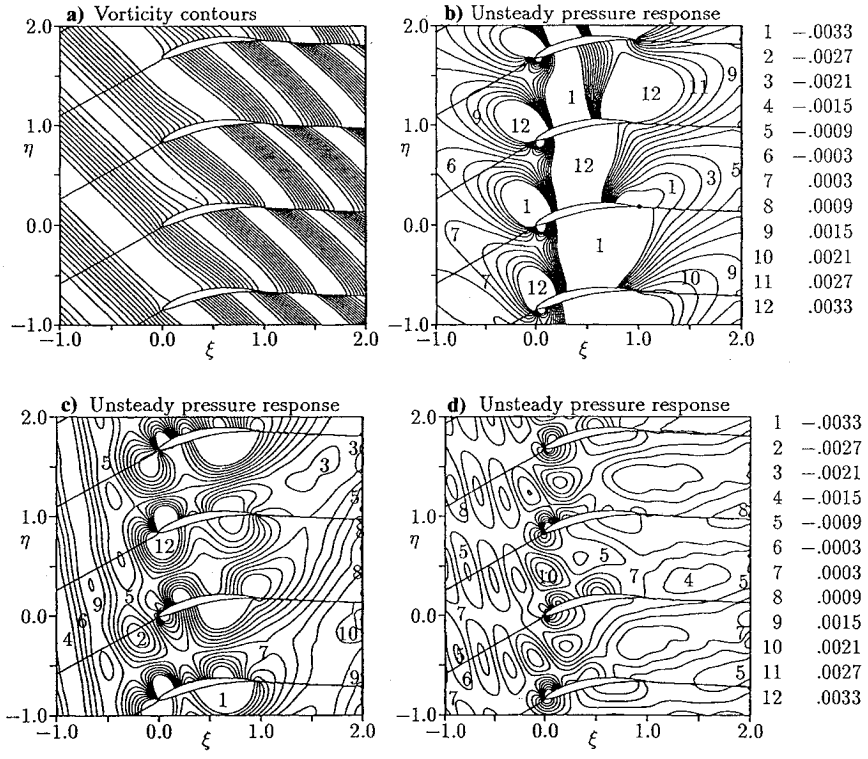

Fig. 4 a) Vortical field at BPF; acoustic fields at b) BPF, c) 2 BPF, and d) 3 BPF.

pressure $\langle \tilde{p}^2 \rangle = p_{\text{rms}}^2$ for a pressure disturbance at frequency ω is defined to be

$$\langle \tilde{p}^2 \rangle = \frac{1}{2\pi}\int_0^{2\pi} \tilde{p}^2 \, \mathrm{d}(\omega t) \tag{24}$$

The acoustic response at a single frequency is composed of a series of individual modes with different wave numbers, i.e.,

$$\tilde{p} = \mathrm{Re}[p \exp(i\omega t)] = \mathrm{Re}\left[\left(\sum_{n=-\infty}^{+\infty} p_n\right)\exp(i\omega t)\right] \tag{25}$$

The complex amplitude of the nth mode p_n can be expressed as

$$p_n = a_n \exp[\beta_n \xi + i(k_{\xi,n}\xi + k_{\eta,n}\eta)] \tag{26}$$

where a_n, β_n, $k_{\xi,n}$, and $k_{\eta,n}$ are the complex amplitude, attenuation constant, axial wave number, and circumferential wave number of the nth mode, respectively. Substituting Eq. (25) into Eq. (24) and performing the averaging result in

$$\langle \tilde{p}^2 \rangle = \frac{1}{4}\sum_{n,m=-\infty}^{+\infty} (p_m p_n^* + p_n p_m^*) = \frac{1}{2}\sum_{n,m=-\infty}^{+\infty} \mathrm{Re}(p_n p_m^*) \tag{27}$$

where the superscript * denotes the complex conjugate. From Eq. (26), the terms in Eq. (27) depend upon circumferential position, and so the sound pressure level based on this quantity is also dependent upon circumferential position. This dependence can be eliminated by averaging $\langle \tilde{p}^2 \rangle$ around the circumference, i.e., integrating from $\eta = 0$ to $\eta = N_B G$, where N_B is the number of blades in the stator row, and dividing by the circumference. The result, substituted into Eq. (23), defines the circumferentially averaged sound pressure level $\overline{SPL}$ and is given by

$$\overline{SPL} = 10\log_{10}\left(\sum_{n=-\infty}^{+\infty}\frac{1}{2}p_n p_n^*\right) - 20\log_{10} p_{\text{ref}} \tag{28}$$

where the overbar indicates circumferential averaging. Neglecting the reference term on the right gives the relative circumferentially averaged sound pressure level $\overline{SPL}_{\text{rel}}$. The argument to the logarithm in Eq. (28) is a function of the length of the acoustic response vector $\boldsymbol{p}_R$, i.e.,

$$\sum_{n=1}^{N}\frac{1}{2}p_{R,n}p_{R,n}^* = \frac{1}{2}\boldsymbol{p}_R^H\boldsymbol{p}_R = \frac{1}{2}\|\boldsymbol{p}_R\|^2 \tag{29}$$

Since the logarithm is a monotonically increasing function, the minimum of its argument corresponds to the minimum of $\overline{SPL}$. Consequently, since the least-squares solution for the control surface motions given in Eq. (20) minimizes $\|\boldsymbol{p}_R\|$, it also minimizes $\overline{SPL}$.

The conclusion is that if the number of acoustic response modes N is equal to the number of independent control surfaces K, then the control surface displacements given by Eq. (17) give complete cancellation. If $K < N$, however, then the magnitude of the net propagating acoustic response vector provides a convenient measure of the net sound and can be minimized by using the least-squares minimization procedure given in Eq. (20) or the weighted least-squares minimization procedure given in Eq. (22). The least-squares minimization procedure also minimizes the circumferentially averaged sound pressure level $\overline{SPL}$.

IV. Results

The following results are based on an analysis of a representative fan stage composed of an upstream fan rotor and a downstream fan exit guide vane. The FEGV blades use a thickness distribution of a NACA 0008 airfoil superimposed on a circular arc camber line whose height at midchord is 0.08. The FEGV has a gap-to-chord ratio G of 0.836 and a stagger angle Θ of 10 deg. The inlet and exit relative freestream Mach numbers are $M_{-\infty} = 0.55$ and $M_{+\infty} = 0.45$, and the inlet and exit flow angles are $\Omega_{-\infty} = 30$ deg and $\Omega_{+\infty} = -2.39$ deg, respectively. The rotor blade passing reduced frequency is $\omega = 4.106$, and the interblade phase angle at BPF is $\sigma = -2.513$. The chord length of the fan blades is approximately 2.3 times that of the FEGV blades. The gap-to-chord ratio G' of the fan rotor is 2.09, nondimensionalized by stator chord, and its exit Mach number and exit flow angle are $M'_{+\infty} = 0.67$ and $\Omega'_{+\infty} = -45$ deg,

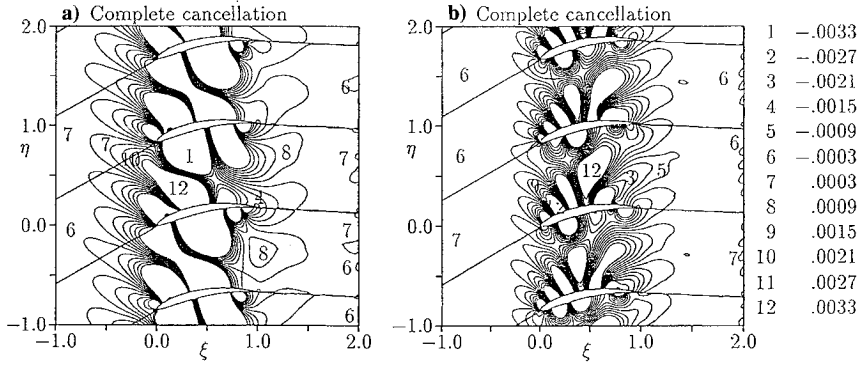

Fig. 5 Acoustic fields showing complete cancellation of propagating modes at a) 2 BPF and b) 3 BPF.

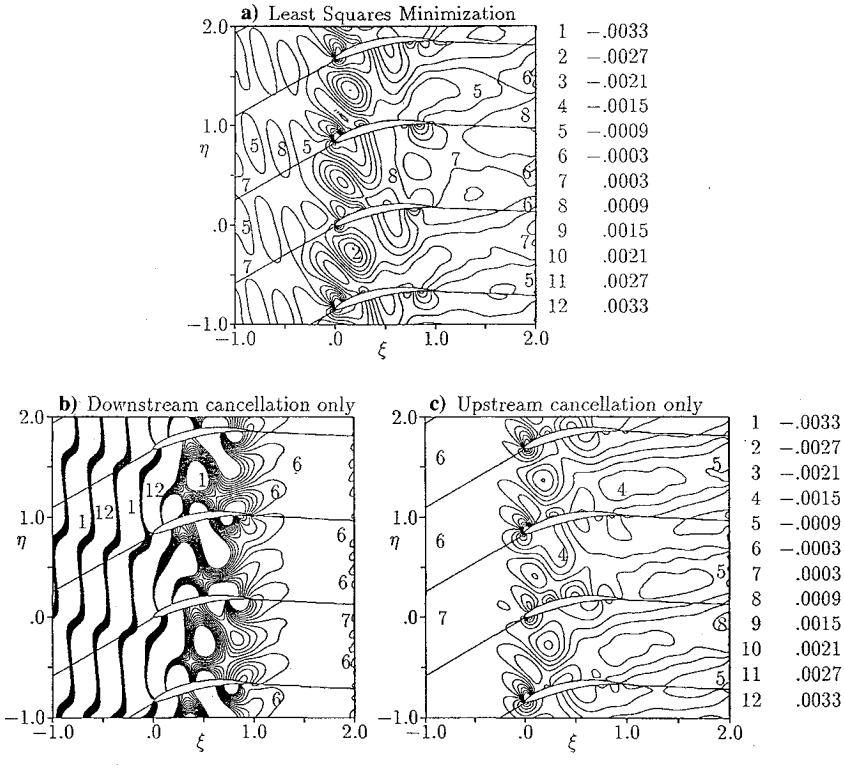

Fig. 6 Weighted least-squares minimizations: a) least-squares solution with two pistons and four modes, b) downstream cancellation only, c) upstream cancellation only.

respectively. The wheel speed at the radial location chosen for the two-dimensional cascade section is 1.366, nondimensionalized with respect to the inlet flow speed to the stator row.

A. Generation

The wake model given in Sec. II.A was used to compute a wake velocity distribution at an axial position two (rotor) blade chords downstream of the rotor, which corresponded to the leading edges of the stator vanes. At that axial location, the wake model yielded $V'_{min}/V'_e = 0.55$, $\delta = 0.288$, and $C_D = 0.032$, as noted in the discussion of Fig. 2. A Fourier decomposition of the velocity field determined the Fourier components of the unsteady excitation at the FEGV inlet. Table 1 shows the v_n^+ values used, along with the frequencies and interblade phase angles for the first three harmonics of the blade passing frequency.

A far-field analysis of the stator row reveals that at BPF all acoustic response modes are "cut off," i.e., they are of decaying type. At 2 BPF, there is one propagating acoustic response mode in each of the upstream and downstream flowfields, and at 3 BPF, there are two in each field. Figure 4 shows the numerical predictions for the real part of the unsteady vorticity at BPF and the real part of the unsteady pressure response at BPF, 2 BPF, and 3 BPF. The vortical fields at 2 BPF and 3 BPF are similar to that at BPF. The vorticity in Fig. 4a is convected through the blade row by the steady background flow. For the acoustic response fields, the contour ranges were chosen to emphasize the propagating acoustic modes. Note that in the BPF acoustic contour plot shown in Fig. 4b the cut-off acoustic modes are illustrated by an unsteady pressure field that decays with increasing distance from the blade row.

The pressure contours for the 2 BPF case in Fig. 4c show single propagating waves upstream and downstream of the cascade. Measuring propagation angles counterclockwise from the positive ξ axis gives −170.8 deg for the upstream acoustic wave and −27.8 deg for the downstream acoustic wave. The wavelengths of the propagating acoustic response waves are 0.676 and 1.98, respectively. The complex amplitude of the upstream propagating wave is $p_{R,-\infty} = (-0.1309 \times 10^{-2}, 0.4937 \times 10^{-3})$, and that of the downstream propagating wave is $p_{R,+\infty} = (0.1970 \times 10^{-2}, -0.2540 \times 10^{-3})$.

The 3 BPF acoustic field in Fig. 4d shows two propagating waves in each flowfield. The upstream waves are propagating at angles of 172.8 deg and −156.5 deg from the positive ξ axis and

have wavelengths of 0.52 and 0.42, respectively. The downstream waves are propagating at angles of 18.7 deg and −79.0 deg and have wavelengths of 1.33 and 1.03. The complex amplitudes of these waves are

$$p_{R,-\infty,1} = (0.2065 \times 10^{-3},\ 0.4054 \times 10^{-3})$$
$$p_{R,-\infty,2} = (-0.5222 \times 10^{-3},\ -0.3309 \times 10^{-3})$$
$$p_{R,+\infty,1} = (0.1135 \times 10^{-3},\ 0.2421 \times 10^{-3}) \quad (30)$$
$$p_{R,+\infty,2} = (0.8927 \times 10^{-3},\ 0.2673 \times 10^{-3})$$

B. Control

Complete Cancellation

To demonstrate complete cancellation of the propagating acoustic modes at each multiple of BPF, the number of control surfaces was chosen to be equal in each case to the known number of propagating acoustic response waves. For this demonstration, the lengths of all of the control surfaces were chosen to be 0.1. The locations of the control surfaces were specified arbitrarily, and as long as nonoverlapping control surfaces were selected, the resulting control matrix $\boldsymbol{A}$ in Eq. (17) was invertible. The elements of $\boldsymbol{A}$ were determined by specifying a unit amplitude displacement for each control surface as an excitation and calculating the resulting complex amplitudes of each of the propagating response modes.

Since two propagating acoustic response modes exist at 2 BPF, two control surfaces (on each blade of the cascade) were selected. One was placed on the suction surface centered at $x = 0.2$; the other, on the pressure surface at $x = 0.8$. The solution to Eq. (17) for the 2 BPF excitation gave the complex amplitudes of the control surface motions as $r_1 = (0.2542 \times 10^{-3}, -0.4153 \times 10^{-3})$ and $r_2 = (-0.1224 \times 10^{-2},\ 0.1080 \times 10^{-2})$.

Four control surfaces were used for the 3 BPF case, two of which were placed on each surface of the blade. The control surfaces on the suction surface were centered at $x = 0.2$ and $x = 0.7$; those on the pressure surface, at $x = 0.3$ and $x = 0.8$. The solution to Eq. (17) then gave

$$r_1 = (0.4286 \times 10^{-4},\ 0.9962 \times 10^{-4})$$
$$r_2 = (0.9207 \times 10^{-5},\ 0.1902 \times 10^{-3})$$
$$r_3 = (0.2665 \times 10^{-3},\ 0.6581 \times 10^{-4}) \quad (31)$$
$$r_4 = (-0.4100 \times 10^{-4},\ 0.1854 \times 10^{-3})$$

Table 2 Least-squares minimization of the net acoustic response, with four propagating acoustic response modes and only two control surfaces

	Magnitudes of each propagating acoustic response mode, $\|p_{R,n}\|$		
n	No control	Control	Change, %
1	0.4550×10^{-3}	0.2738×10^{-3}	−39.8
2	0.6182×10^{-3}	0.3931×10^{-3}	−36.4
3	0.2674×10^{-3}	0.2872×10^{-3}	+7.40
4	0.9319×10^{-3}	0.6876×10^{-3}	−26.2

Table 3 Weighted least-squares minimization cancelling the downstream acoustic response modes

	Downstream cancellation only, $\|p_{R,n}\|$		
n	No control	Control	Change, %
1	0.4550×10^{-3}	0.1404×10^{-1}	+2986
2	0.6182×10^{-3}	0.8098×10^{-2}	+1210
3	0.2674×10^{-3}	0.2066×10^{-6}	−99.92
4	0.9319×10^{-3}	0.3232×10^{-6}	−99.97

Table 4 Weighted least-squares minimization cancelling the upstream acoustic response modes

	Upstream cancellation only, $\|p_{R,n}\|$		
n	No control	Control	Change, %
1	0.4550×10^{-3}	0.1165×10^{-6}	−99.95
2	0.6182×10^{-3}	0.2156×10^{-6}	−99.97
3	0.2674×10^{-3}	0.2001×10^{-3}	−24.98
4	0.9319×10^{-3}	0.9989×10^{-3}	+7.190

for the complex amplitudes of the control surface motions. The magnitudes of the acoustic response waves when the vortical excitation and the control surface motions were both present were all on the order of 10^{-7}. By way of reference, for a typical FEGV chord of 6–12 in. this implies a required actuator displacement on the order of a few thousandths of an inch or less.

Contour plots of the acoustic fields with the control motions applied along with the vortical excitation are shown in Fig. 5. Though the response within the blade row in these figures is dramatically larger than that without the control motions, the far-field acoustic response has been essentially eliminated. It should be noted that no other structural or aerodynamic effects due to the piston motions have been evaluated. The control analysis could be performed with the pistons at alternate locations, however, should this be necessary.

Least Squares Minimization

To illustrate the effects of the least-squares minimization solution given in Eq. (20) and the weighted least-squares solution given in Eq. (22), consider the same 3 BPF case as given earlier in which there are four propagating acoustic response waves. Assume now that only two pistons are available for control. The two pistons selected for demonstration of the least-squares concept are the ones used to achieve complete cancellation for the 2 BPF excitation. In that case, the pistons each had length 0.1 and were centered at $x = 0.2$ on the suction surface and $x = 0.8$ on the pressure surface, respectively.

The least squares minimization resulting from Eq. (20) yields the complex amplitudes $r_1 = (-0.4830 \times 10^{-5},\ -0.4022 \times 10^{-4})$ and $r_2 = (-0.7891 \times 10^{-4},\ -0.8567 \times 10^{-5})$. The acoustic contours for this case are shown in Fig. 6a. With the control applied, the changes in the magnitudes of each propagating response wave are shown in Table 2. The magnitude of the net propagating response vector $\|\boldsymbol{p}_R\|$ has been reduced by 28.4% overall, which corresponds to a decrease in the circumferentially averaged *SPL* of about 3 dB.

To demonstrate the weighted least-squares minimization procedure, a weighting matrix is chosen that required complete cancellation of both downstream modes. The required control displacements that result are $r_1 = (-0.5216 \times 10^{-3},\ 0.3196 \times 10^{-3})$ and $r_2 = (-0.2631 \times 10^{-3},\ 0.2343 \times 10^{-3})$. Acoustic contours for this case are shown in Fig. 6b. Note that the downstream flowfield is essentially completely quiet, whereas the upstream acoustic response has been increased significantly. The results are summarized in Table 3.

These results are dramatic, in that the downstream acoustic response waves have been virtually eliminated but the magnitudes of the upstream response waves have increased by almost two orders of magnitude. The reason for this is that the sensitivity of the downstream acoustic response waves to control surface oscillations is less than that of upstream response waves. A relatively large control displacement is thus required to achieve a large enough response to cancel the undesired downstream modes. This large control surface displacement is then multiplied by the far greater sensitivity of the upstream modes to yield a strong acoustic response upstream.

This suggests that if the weighting matrix is chosen so that only the upstream modes are canceled rather than the downstream modes, the overall result will not be as severe. Application of the control analysis reveals that this is indeed the case, and acoustic

contours for this case are shown in Fig. 6c. The required control displacements in this case are $r_1 = (-0.1293 \times 10^{-4}, -0.3205 \times 10^{-4})$ and $r_2 = (-0.3094 \times 10^{-4}, 0.3616 \times 10^{-4})$, and the changes in the response modes are shown in Table 4.

The upstream response modes respond more readily to the control, and this is reflected in the fact that even though the downstream modes were ignored in the weighted analysis in this case, one of them actually decreased in magnitude by almost 25%.

The conclusion to be drawn, therefore, is that in each case where control is to be applied and there are not enough pistons available for complete cancellation, it is important to examine the behavior of all propagating acoustic response modes to the control.

V. Conclusions

The purpose of this investigation has been to assess the potential of antisound generation by oscillating blade surface actuators. To do so, an existing rotor wake model was analyzed to determine representative vortical excitations to a downstream FEGV, and the subsequent acoustic responses of the FEGV were computed using the LINFLO analysis. Blade surface actuators were implemented as sections of the stator blades executing translational oscillations perpendicular to the stator blade surfaces, at complex amplitudes found from the solution of a linear system of equations.

If the number of available control surfaces is equal to the number of propagating acoustic response waves, this system of equations can be solved exactly, resulting in a set of control displacements that completely cancel the noise. If the number of acoustic response waves exceeds the number of control surfaces, then the magnitude of a net acoustic response vector can be minimized via a least-squares minimization procedure. This provides a convenient measure of the control effectiveness, as the magnitude of the acoustic response vector is directly related to the circumferentially averaged sound pressure level. A weighting matrix was also included in the control analysis to allow selective cancellation of the acoustic response waves.

For the representative fan stage under consideration, the required control surface displacements to minimize the noise ranged from a few ten-thousandths to a few thousandths of stator chord. This result is promising, indicating the possibility of designing actuators to execute the required motions. It should be cautioned, however, that no other structural or aerodynamic effect of the control surface motions has been examined. The conclusion, therefore, is that the use of antisound generation by blade surface actuators has been shown in the present analytical/computational study to be a promising approach, and no results were found that preclude the possibility of a successful implementation of this technique.

References

[1]Simonich, J., Lavrich, P., Sofrin, T., and Topol, D., "Active Aerodynamic Control of Wake-Airfoil Interaction Noise—Experiment," DGLR/AIAA Paper 92-02-038, May 1992.

[2]Thomas, R., Burdisso, R., Fuller, C., and O'Brien, W., "Active Control of Fan Noise from a Turbofan Engine," AIAA Paper 93-0597, Jan. 1993.

[3]Ffowcs Williams, J., "Anti-Sound," *Proceedings of the Royal Society of London, Series A, Mathematical and Physical Sciences,* Vol. 395, No. 1808, 1984, pp. 63–88.

[4]Koopmann, G., and Fox, D., "Active Source Cancellation of the Blade Tone Fundamental and Harmonics in Centrifugal Fans," *Journal of Sound and Vibration,* Vol. 126, No. 2, 1988, pp. 209–220.

[5]Cunefare, K., and Koopman, G., "Global Optimum Active Noise Control: Surface and Far Field Effects," *Journal of the Acoustic Society of America,* Vol. 90, No. 1, 1991, pp. 365–373.

[6]Meirovitch, L., and Thangjitham, S., "Active Control of Sound Radiation Pressure," *ASME Transactions, Journal of Vibration, Acoustics, Stress and Reliability in Design,* Vol. 112, No. 2, 1990, pp. 237–244.

[7]Neise, W., and Koopmann, G., "Active Sources in the Cutoff of Centrifugal Fans to Reduce the Blade Tones at Higher-Order Duct Mode Frequencies," *ASME Transactions, Journal of Vibration and Acoustics,* Vol. 113, No. 1, 1991, pp. 123–131.

[8]Kerschen, E. J., "Active Aerodynamic Control of Wake-Airfoil Interaction Noise—Theory," DGLR/AIAA Paper 92-02-039, May 1992.

[9]Verdon, J. M., "Review of Unsteady Aerodynamic Methods for Turbomachinery Aeroelastic and Aeroacoustic Applications," *AIAA Journal,* Vol. 31, No. 2, 1993, pp. 235–250.

[10]Hall, K. C., and Verdon, J. M., "Gust Response Analysis for Cascades Operating in Nonuniform Mean Flows," *AIAA Journal,* Vol. 29, No. 9, 1991, pp. 1463–1471.

[11]Majjigi, R. K., and Gliebe, P. R., "Development of a Rotor Wake/Vortex Model," NASA CR-174849, June 1984.

[12]Verdon, J. M., "The Unsteady Flow in the Far Field of an Isolated Blade Row," *Journal of Fluids and Structures,* Vol. 3, No. 2, 1989, pp. 123–149.

[13]Caspar, J. R., "Unconditionally Stable Calculation of Transonic Potential Flow Through Cascades Using an Adaptive Mesh for Shock Capture," *Transactions of ASME A: Journal of Engineering for Power,* Vol. 105, No. 3, 1983, pp. 504–513.

[14]Goldstein, M. E., "Unsteady Vortical and Entropic Distortions of Potential Flows Round Arbitrary Obstacles," *Journal of Fluid Mechanics,* Vol. 89, No. 3, 1978, pp. 433–468.

[15]Atassi, H. M., and Grzedzinski, J., "Unsteady Disturbances of Streaming Motions Around Bodies," *Journal of Fluid Mechanics,* Vol. 209, Dec. 1989, pp. 385–403.

[16]Strang, G., *Linear Algebra and Its Applications,* Academic Press, New York, 1980, pp. 112–115.